RESEARCH PAPER

Computational And In-Vitro Evaluation Of Turmeric Oleoresin As An Mmp-9 Inhibitor For Wound Healing

Vijay Aadhithya C[1], Shunmuga Priya Velu[2]*

[1,2]*Department of Biotechnology, Sethu Institute of Technology, Pulloor, Virudhunagar-626 115, Tamil Nadu, India*

*Email- shunmu30@gmail.com**

ABSTRACT

Diabetes affects over 500 million people worldwide, with high incidence in Southeast Asia, particularly India. Diabetic wound healing affect 1 in 3 to 5 diabetic individuals, often leading to non-healing wounds, infections, hospitalization, and amputations. Current treatment methods fail to address the multifactorial pathology of chronic diabetic wounds, particularly prolonged inflammation and extracellular matrix (ECM) degradation. The complicated process of wound healing includes ECM remodelling, inflammatory decrease, and coordinated tissue regeneration. This process could be clogged by overexpression of matrix metalloproteinase-9 (MMP-9), an enzyme that breaks down extracellular matrix. The purpose of this study is to investigate ar turmerone and turmerone's potential for wound healing, particularly its capacity to inhibit MMP-9 by combining *in vitro* and *in silico* approaches. Molecular docking showed strong MMP-9 binding, with turmerone displaying a better docking score (-10.1 kcal/mol) than ar-turmerone (-8.1 kcal/mol). Gas chromatography mass spectrometry (GC-MS) analysis of fresh C. longa rhizome oil confirmed the presence of both compounds in turmeric oil, with turmerone comprising 34.93% of the extract. *In vitro* scratch assays using L929 fibroblast cells proved that the two compounds both accelerate cell proliferation and migration in a dose-dependent fashion, signifying their efficiency in healing wound closure. These results infer that turmerone can act as potential natural therapeutic drugs in accelerating wound healing through MMP-9 inhibition.

Keywords: Diabetic Wound, MMP-9 inhibitor, Turmerone, Computational analysis, Scratch assay.

How to cite this article: Vijay Aadhithya C, Shunmuga Priya Velu. Computational and In-Vitro Evaluation of Turmeric Oleoresin as an MMP-9 Inhibitor for Wound Healing. Int J Drug Deliv Technol. 2026;16(23s): 494-508. DOI: 10.25258/ijddt.16.23s.54

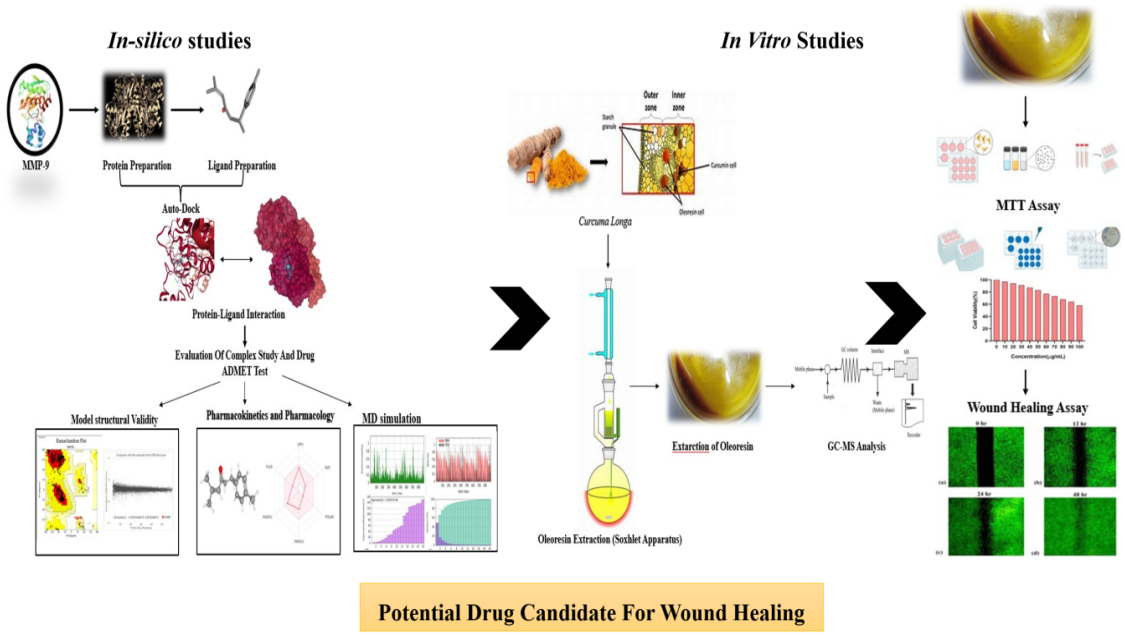

Fig: Graphical abstract

INTRODUCTION

Diabetes mellitus is a chronic metabolic disorder caused by defects in insulin secretion, insulin action, or both, and is associated with hyperglycemia and disturbances in carbohydrate, fat, and protein metabolism (1). According to the International Diabetes Federation (IDF) estimates in 2020, 88 million individuals in Southeast Asia, including 77 million in India, had diabetes (2). Early diagnosis, effective treatment, and lifestyle changes are essential for the management of the disease. Nevertheless, current interventions like insulin treatment and oral antidiabetic drugs are limited by drug resistance, side effects, and systemic toxicity (3). Therefore, there is an increasing focus on discovering alternative therapeutics, especially from medicinal plants.

A significant complication of diabetes is the development of chronic non-healing wounds, most notably diabetic foot ulcers (DFUs). Worldwide, more than 500 million individuals suffer from diabetes, and of those, one in three to five are prone to developing DFUs (4). These ulcers are associated with high recurrence rates, hospitalization, and amputation of the limbs. Impaired healing in diabetic patients' results from chronic inflammation, oxidative stress, failure of angiogenesis, neuropathy, and aberrant neuropeptide signaling5. Additionally, reduced production of growth factors, defective collagen deposition, and dysregulation of extracellular matrix (ECM) remodelling also hinder wound healing (6), (7).

Wound healing occurs in three overlapping phases: inflammation, proliferation, and remodeling. In diabetic wounds, the inflammatory phase is prolonged and the proliferative response is defective, leading to chronic ulcers (8). Medicinal plants have shown considerable promise in accelerating healing and reducing the risk of limb amputation in DFUs (9).

Matrix metalloproteinases (MMPs) are zinc-dependent endopeptidases critical for ECM remodeling. These include collagenases, gelatinases, stromelysins, and aggrecanases, regulated by tissue inhibitors of metalloproteinases (TIMPs) 10. Among these, MMP-9 plays a central role in wound healing. In diabetic ulcers, MMP-9 is often overexpressed, with an excess of ECM degradation, impairment in tissue regeneration, and delayed wound closure (11). Regulatory pathways such as NF-κB and Notch1 that regulate MMP-9 expression and are being explored as therapeutic targets for diabetic wounds (12). Despite the fact that multiple treatment modalities such as growth factors, stem cell therapy, and gene therapy are available, their effective management of DFUs is difficult to achieve due to antimicrobial resistance, and clinical limitations (13).

Turmeric (Curcuma longa), which is widely used in traditional medicine, exhibits a strong anti-inflammatory, antioxidant, and antimicrobial activity. Curcumin, its principle bioactive component has been demonstrated to possess vast therapeutic potential to heal wounds (14). Turmeric oleoresin, a lipid-soluble fraction that contains high levels of curcuminoids as well as essential oil, offers greater bioavailability and sustained therapeutic effects compared to isolated curcumin (15), (16). Turmeric oleoresin is, however, limited by poor water solubility and susceptibility to degradation. For this purpose, novel delivery systems such as hydrogels, nanoemulsions, and nanofiber scaffolds are being developed to enhance its bioactivity and therapeutic efficacy in chronic wound healing (17), (18).

MATERIALS AND METHODS

In-silico Studies

Selection of protein and Ligands

Different structural forms of the MMP-9 protein were obtained from the Protein Data Bank (PDB). From these, the most optimal structure was selected based on the experimental method, resolution, and the presence or absence of mutations. A high-resolution structure, specifically one with a resolution of 2.0 Å, was preferred. Ligand structures were retrieved from reputable databases such as PubChem, ensuring that proper stereochemistry and complete molecular configurations were maintained. A ligand was chosen based on compliance with Lipinski's Rule of Five, including a molecular weight between 150 and 500 Da, a logP value of ≤5, and a polar surface area of ≤90 Å² (19).

Preparation of Protein

Proteins were prepared in Chimera through a series of critical steps to ensure a clean and optimized structure. The process was initiated by loading the PDB file to check for missing residues or structural issues. Unwanted components, such as water molecules and ions, were removed. Atoms or hydrogen atoms necessary to complete the molecular structure were added using Dock Prep. Structural errors were resolved by

eliminating steric clashes using the Find Clashes/Contacts tool. Appropriate charges, such as AMBER or Gasteiger, were assigned to the structure using the Add Charge tool. Energy minimization of the geometry was then performed using the Minimize Structure tool. Finally, the prepared protein was saved in PDB format for further computational analysis (20), (21).

Quality Evaluation of the Model

Homology modeling was employed to construct the 3D structure of the target protein, which was subsequently validated using various computational tools. A Ramachandran plot was generated by PROCHECK to verify the stereochemical quality, and a quality score based on structural parameters was provided by QMEAN. The atomic model's consistency with its sequence was assessed by Verify3D, while non-bonded atomic interactions were evaluated by ERRAT. Finally, the overall quality of the model was aligned with experimentally solved structures by estimating the Z-score using ProSa-Web. All of these validation methods were utilized to ensure the accuracy and reliability of the predicted model (22).

SWISS ADME Properties

The Swiss ADME submission page allows users to input a list of SMILES for molecular analysis. SwissADME employs various computational methods optimized for speed, robustness, and interpretability to assess pharmacokinetic profiles, making it accessible even to non-experts. It offers unique methods like iLOGP and the BOILED-Egg alongside multiple predictions for parameters, providing a comprehensive tool for drug design and assessment in comparison to existing platforms (23).

Toxicity Prediction

The ProTox 3.0 platform features seven classification steps: (i) acute toxicity, (ii) organ toxicity, (iii) toxicological endpoints, (iv) toxicological pathways, (v) molecular initiating events, (vi) metabolism, and (vii) toxicity targets, with a total of 61 models, including 28 new ones developed using Random Forest (RF) and Deep Learning algorithms. These models utilize two molecular fingerprints: MACCS and Morgan circular. Models were evaluated based on accuracy, sensitivity and specificity, with a range from 0 to 1. The best-performing model for each endpoint was saved using pickle and implemented in ProTox 3.0. Different toxicity models were constructed, including acute toxicity, hepatotoxicity, neurotoxicity, and nephrotoxicity. The acute toxicity model focused on chemical similarities, while hepatotoxicity and neurotoxicity were based on previous methodologies (24).

Molecular Docking studies

Receptor–ligand docking was performed using PyRx software integrated with AutoDock Vina. PDB/MOL2 files were converted to PDBQT format. The receptor and ligands were prepared using AutoDock Tools, and the Lamarckian genetic algorithm was employed for the docking process. In PyRx, binding affinity calculations were carried out, and the results were saved for further analysis. Binding interactions were visualized using Discovery Studio, by which datasets of ligands were efficiently screened for potential interactions with the target receptors (25), (26).

MD Simulations

Molecular dynamics (MD) simulations of protein–ligand complexes were conducted using the iMOD server (iMODS) (http://imods.chaconlab.org), a tool for analyzing macromolecular flexibility and stability. Molecular movements were simulated, and conformational stability was evaluated. To assess the protein–TMZ complex dynamics, deformability, B-factor, eigenvalues, variance, covariance maps, and elastic network models were analyzed. Docked PDB structures were submitted to iMODS with default parameters to ensure standardization. Critical residues involved in ligand binding and stability were identified through simulation results, offering insights into binding mechanisms and supporting therapeutic design (27).

Extraction of Turmeric Oleoresin

Turmeric oleoresin was extracted from fresh and dried Curcuma longa rhizomes using a Soxhlet apparatus. Dried rhizomes were processed into powder after drying at 40°C–50°C, while fresh rhizomes were cleaned, peeled, and ground into a paste. Approximately 25–50 g of dried powder or muslin-wrapped paste was placed in the extraction chamber, and 300 mL of 95% ethanol was used as the solvent. Upon heating at 60°C–70°C, curcuminoids and volatile compounds were extracted continuously 26. Extraction was considered complete when the siphoning solvent turned clear after 4–6 hours. Following extraction, ethanol was evaporated

by heating, and the concentrated oleoresin—appearing as a semi-solid—was filtered and further dried using a rotary evaporator under reduced pressure or a hot air oven at 40°C. To prevent degradation, the final extract was stored in amber airtight containers at under refrigeration (27). Chemical profiling was performed using GC-MS to determine purity and confirm the presence of bioactive compounds, ensuring the extract's quality and efficacy (28).

Characterization of turmeric oleoresin

Pre-characterization of turmeric oleoresin, a bioactive compound extracted from turmeric rhizomes, was conducted using UV-Vis spectroscopy for preliminary detection, while precise identification and quantification were carried out using Gas Chromatography–Mass Spectrometry (GC-MS). Dried turmeric rhizomes were extracted with hexane or ethyl acetate, followed by filtration through a 0.22 µm membrane filter. The UV-Vis spectrum of the extract was recorded within the 200–500 nm range, and a characteristic absorption peak between 250–280 nm, indicative of turmerones, was observed. The concentrations of ar-turmerone and turmerone were estimated using a calibration curve constructed with standard solutions (29).

GC-MS Analysis

Gas Chromatography-Mass Spectrometry (GC-MS) was utilized to identify and quantify ar-turmerone and turmerone, bioactive compounds found in turmeric oleoresin. Analysis was conducted using an Agilent GC 7890A / MS 5975C system equipped with a DB-5MS capillary column (30 m × 0.25 mm ID × 0.25 µm film thickness). Turmeric essential oil was extracted using hexane or ethyl acetate, then filtered through a 0.22 µm membrane. Injection was performed in split mode (10:1) with a 1 µL volume, and the injector temperature was maintained at 250°C. Helium (99.999% purity) served as the carrier gas at a constant flow rate of 1.0 mL/min. The oven temperature was initially set at 60°C (held for 2 min), ramped to 180°C at 10°C/min (held for 2 min), and then to 280°C at 5°C/min (held for 5 min), yielding a total run time of approximately 35–40 minutes (29), (30).

***In vitro* Approaches**

MTT Assay

The cytotoxicity of turmeric oleoresin was evaluated using the L929 murine fibroblast cell line. The test compound, prepared in two-fold dilutions, was cultured in DMEM supplemented with penicillin, streptomycin, and 10% inactivated fetal bovine serum. Cells were seeded into 96-well plates and incubated for 24 hours before treatment. Afterwards, 100 µl of each test concentration and MTT reagent were added to each well, followed by a 4-hour incubation at 37°C to allow formazan crystal formation. Absorbance at 590 nm was measured using a Tecan plate reader. IC_{50}, cell viability, and inhibition percentages were calculated using GraphPad Prism 6 through nonlinear regression of a sigmoidal dose-response curve. Cytotoxic effects were quantitatively assessed, revealing insights into the compound's biological activity against L929 cells (31).

Wound Healing Assay

Cells were detached using standard passaging procedures. A six-well plate was prepared with 1–2 mL of pre-warmed media per well. Cells were seeded in 24-well plates at 4000 cells/well and incubated at 37°C for 24 hours. Samples at IC_{50} concentrations were then added at 50 µg/mL. After 18–24 hours, once confluence was reached, a straight-line scratch was made using a cell scriber. Detached cells were removed by gentle washing, and fresh medium was added. Cells were immediately imaged using a fluorescence microscope (Olympus CKX-53, Japan). Acridine Orange staining was used to visualize live cells and nuclear morphology (32).

RESULT

Selection of Protein and Ligands

Selection of Protein

Retrieving MMP-9 structures from the Protein Data Bank (PDB) is the initial step in choosing the most suitable protein structure for AutoDock. Next, the quality of the protein is assessed by removing truncated entries, ranking structures by resolution, and ensuring the preservation of critical motifs, such as the catalytic zinc-binding site. Once the optimal structure PDB ID 5TH6 is identified (Fig. 1a), it is prepared for docking by removing heteroatoms and water molecules using software such as ChimeraX, adding missing hydrogens, setting the active site and docking grid, and energy minimization with software such as PyRx.

Selection of Ligands

To select appropriate ligands for AutoDock, complete structures with correct stereochemistry were obtained from authentic databases such as PubChem. Ligands were chosen based on drug-likeness according to Lipinski's Rule of Five, which includes criteria such as logP (≤ 5) and molecular weight (150–500 Da). The number of rotatable bonds in each ligand was calculated to assess flexibility and ensure suitability for docking. To identify ligands with higher potential for wound healing, preliminary docking trials were conducted to evaluate binding affinity. Additionally, tools like SwissADME were used to assess ADMET properties, predicting bioavailability and potential toxicity. Finally, the selected ligands were converted to PDBQT format using AutoDock Tools to prepare them for docking.

Retrieval of Protein and Ligands

The selected protein and ligands for AutoDock were obtained by accessing the RCSB Protein Data Bank (PDB) website, selecting the PDB format, and downloading the human matrix metalloproteinase-9 (MMP-9) structure with PDB ID 5TH6 (Fig. 1a). Turmerone and ar-turmerone (Fig. 1b, 1c) were retrieved from PubChem to ensure correct stereochemistry and molecular arrangement. After downloading, the ligands were converted to the PDBQT format using AutoDock Tools to make them compatible with AutoDock. Accurate preparation and acquisition of these compounds were critical for reliable docking studies and binding affinity analysis.

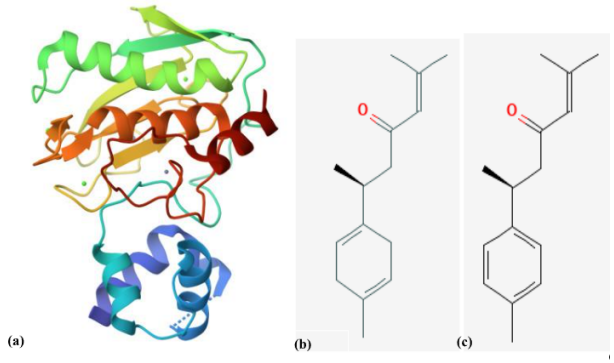

Fig. 1: Structure of protein & Ligand (a) 3D structure of protein (MMP-9); (b) chemical structure of ligand (ar-turmerone); and (c) chemical structure of ligand (Turmerone)

Model Analysis and Quality Evaluation

PROCHECK, Verify 3D, ERRAT, and QMEAN were employed to assess the quality of the predicted three-dimensional protein structure. According to PROCHECK, 95.2% of amino acid residues in the Ramachandran plot fell within the most favoured region. Verifying 3D analysis showed that 93.90% of residues achieved an average 3D-1D score ≥ 0.1, indicating good structural compatibility. The ERRAT tool estimated the model's quality factor at 87.5453, signifying reliable structural accuracy. QMEAN placed the model in the dark grey zone, with a QMEAN4 score of 0.96, suggesting acceptable quality. Additionally, ProSA analysis yielded a Z-score of -6.84, confirming that the model fell within the range of high-quality native protein structures (Fig. 2).

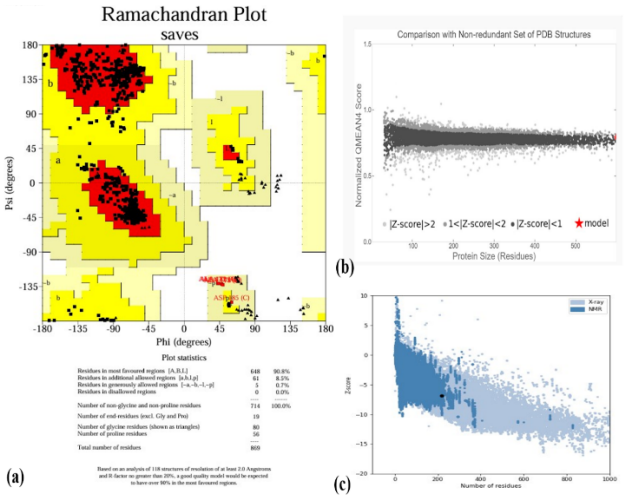

Fig 2: Evaluation of models quality: (a) Ramachandran plot of model structure validated by PROCHECK program; (b) Graphical representation of QMEAN result of the model structure (indicates good agreement between model structure and experimental structures similar size; and (c) Z- score of the protein using proSA server.

Drug Likeness Property

The two bioactive molecules, 1 and 2, were subjected to *in silico* ADME (absorption, distribution, metabolism, excretion) prediction using SwissADME to estimate their overall pharmacokinetic behaviour (Table 1). The drug-likeness of the compounds was assessed based on Lipinski's Rule of Five (Ro5), which focuses on the following criteria: molecular weight less than 500 Daltons, lipophilicity (octanol–water partition coefficient, logP) less than 5, fewer than 10 hydrogen bond donors, and fewer than 5 hydrogen bond acceptors. Both compounds were found to satisfy Lipinski's Ro5.

Table 1: Drug likeness Properties of Selected Phytocompounds

Lipkin's rule of 5	Std value	Ar-turmerone	Turmerone
Molecular weight	<500	216.32 g/mol	216.32 g/mol
H-Bond Donor	<5	0	0
H-Bond acceptor	<10	1	1
Rotable bonds	<10	4	4
Lipophilicity (logP)	<5	3.98	3.37

Toxicity Prediction

The phytocompounds Ar-Turmerone and Turmerone were evaluated for toxicity using computational predictions, likely via ProTox 3. Both compounds showed low risk for general toxicity, demonstrating inactivity against targets such as hepatotoxicity, neurotoxicity, and nephrotoxicity. Ar-Turmerone was classified in toxicity class 4 with a predicted LD_{50} of 2920 mg/kg, while Turmerone was in class 5 with an LD_{50} of 2000 mg/kg. Although these *in silico* results indicate low toxicity, experimental validation is necessary, as prediction accuracy depends on the model and toxicity may vary with dose and exposure. Further studies are required to fully characterize their toxicological profiles.

Table 2: Toxicity profiling of selected phytocompounds

Ligands	Ar-turmerone	Turmerone
Hepatotoxicity	Inactive	Inactive
Neurotoxicity	Inactive	Inactive
Nephrotoxicity	Inactive	Inactive
Respiratory toxicity	Inactive	Inactive
Cardiotoxicity	Inactive	Inactive
Carcinogenicity	Inactive	Inactive
Immunotoxicity	Inactive	Inactive
Mutagenicity	Inactive	Inactive

Molecular Docking

Molecular docking, a widely used computational method to estimate the binding affinity and pose of small molecules with target proteins 33, was employed using PyRx in this study. The binding abilities of Turmerone and ar-Turmerone to a wound healing-related target protein were assessed. Turmerone exhibited a more negative docking score (-10.1) compared to ar-Turmerone (-8.1), indicating a higher predicted binding affinity (Table 3). This difference is likely attributable to variations in their molecular structures influencing interactions within the protein's binding site (Fig. 3).

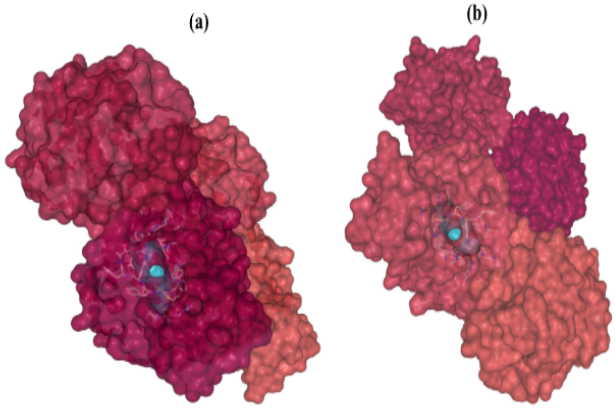

Fig. 3: (a) Molecular docking of ar-turmerone and active site of MMP-9; (b) Molecular Docking of turmerone and active site of MMP-9

Table 3: Protein Ligand Auto dock Score Using Pyrx

Ligand	Binding Affinity
Turmerone	-10.1
ar-Turmerone	-8.1

Protein Ligand Interaction

Turmerone and ar-Turmerone demonstrated strong binding affinities to MMP9, with distinct binding modes for each compound. Turmerone showed a higher affinity (-10.1 kcal/mol) compared to ar-Turmerone (-8.1 kcal/mol), likely due to a pi–pi stacking interaction with His-401, which was absent in ar-Turmerone's binding (Fig. 4 and Fig. 5). Additionally, Turmerone formed a more extensive network of Van der Waals interactions. Further studies are required to clarify the contributions of these interactions to binding affinity and to explore potential differences in their inhibitory mechanisms. Comparison with known MMP9 inhibitors could reveal unique binding strategies. Both compounds exhibited multiple interaction types, suggesting stable complexes with MMP9; however, molecular dynamics simulations

and binding free energy calculations are necessary for a detailed assessment of their dynamic stability and comparative efficacy (34).

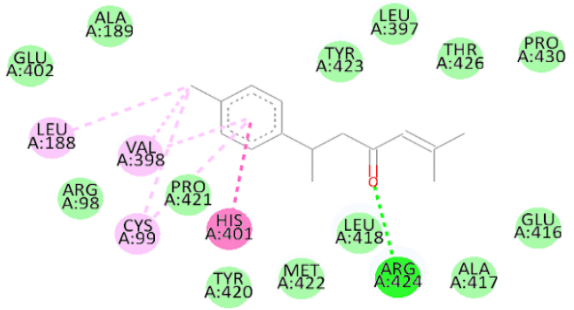

Fig. 4: Turmerone binds with the active site of MMP9

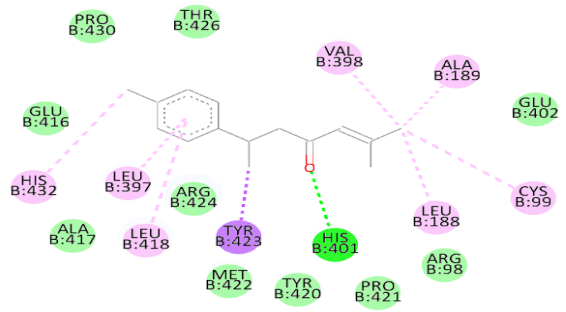

Fig. 5:ar-Turmerone Binds with the active site of MMP9

MD Simulation Studies

The B-factor and deformability plots of the MMP9-Turmerone and MMP9-ar-Turmerone complexes revealed regions of high flexibility, indicated by peak values. The B-factor plots compared experimental PDB data with normal mode analysis (NMA), highlighting stability and flexibility across the protein. Variance inversely correlated with normal modes, with purple and green bars representing individual and cumulative variance, respectively. Larger eigenvalues corresponded to greater rigidity, while smaller values indicated increased flexibility. Covariance matrices illustrated residue correlations, where red indicated strong correlation, white uncorrelated motion, and blue anticorrelation. Higher correlation suggested greater complex stability, critical for understanding protein-ligand dynamics. The elastic network models further highlighted atomic associations, with darker grey regions denoting stiffer, more rigid protein segments (Fig. 6 and Fig. 7). Both complexes exhibited elastic network maps consistent with acceptable structural stability, suggesting that Turmerone and ar-Turmerone influence MMP9 flexibility and dynamics differently.

Extraction of Turmeric Oleoresin

To obtain turmeric oleoresin from turmeric rhizome, begin by preparing the powder from dry and fresh rhizomes and putting it in a thimble. A Soxhlet apparatus is assembled with 200-300 ml of ethanol in the round bottom flask. The solvent is heated to evaporate, condense, and fall into the powder, repeating this process until the powder turns colourless. This procedure separates the turmeric oleoresin from fresh and dried rhizome.

GC-MS Analysis

GC-MS analysis of dry turmeric rhizome oleoresin identified 213 compounds, with turmerone as the major component (41.44%) and ar-turmerone present at 0.14%, indicating that drying significantly altered the composition by reducing ar-turmerone levels. In contrast, fresh turmeric rhizome oleoresin contained 32 compounds, with turmerone (34.93%) and ar-turmerone (8.80%) as the primary constituents. The higher content of turmerone and ar-turmerone in fresh oleoresin supports its selection for further *in vitro* studies due to its potentially greater bioactivity and stability compared to the dried form (Fig. 8 and Fig. 9).

In-vitro studies

MTT Assay

The MTT assay demonstrated that turmeric oleoresin exhibited low cytotoxicity against L929 fibroblast cells, with an $IC_{50} \geq 100$ µg/mL. Cell viability showed a dose-dependent decline, recording 97%, 77%, and 58% viability at 10, 50, and 100 µg/mL concentrations, respectively. The IC_{50} value exceeding 100 µg/mL indicates negligible cytotoxic effects at lower concentrations, confirming the compound's biocompatibility and suitability for subsequent wound healing investigations (Fig. 10,11). These findings corroborate the oleoresin's potential therapeutic application with minimal adverse effects on cellular viability.

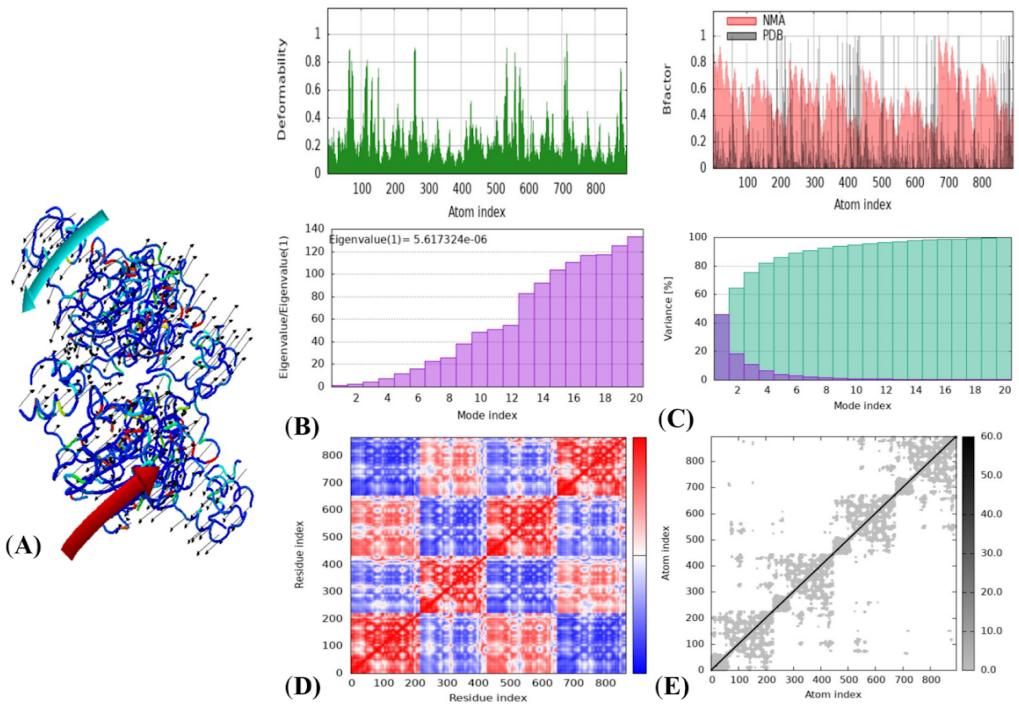

Fig. 6 - MD Simulations of Turmerone (a) Molecular Mobility Evaluated by NMA of the Docked Complexes MMP9 and Turmerone: Outputs of Molecular Dynamics Simulations in Imods for SLIT1-TMZ: (b) Deformability and B-Factor Plot; (c) Eigenvalue and Variance Plot; (d) Elastic Network Model; and (e) Covariance Map

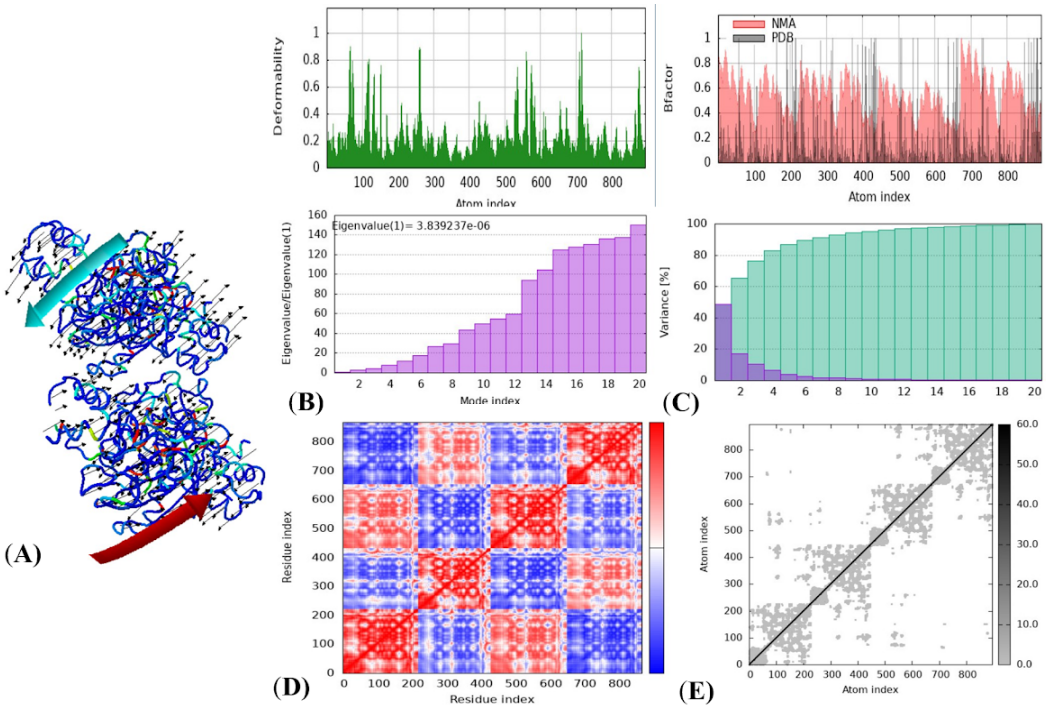

Fig. 7 - MD Simulations of ar-Turmerone (a) Molecular Mobility Evaluated by NMA of the Docked Complexes MMP9 and ar-Turmerone: Outputs of Molecular Dynamics Simulations in Imods for SLIT1-TMZ; (b) Deformability and B-Factor Plot; (c) Eigenvalue and Variance Plot; (d) Elastic Network Model; and (e) Covariance Map.

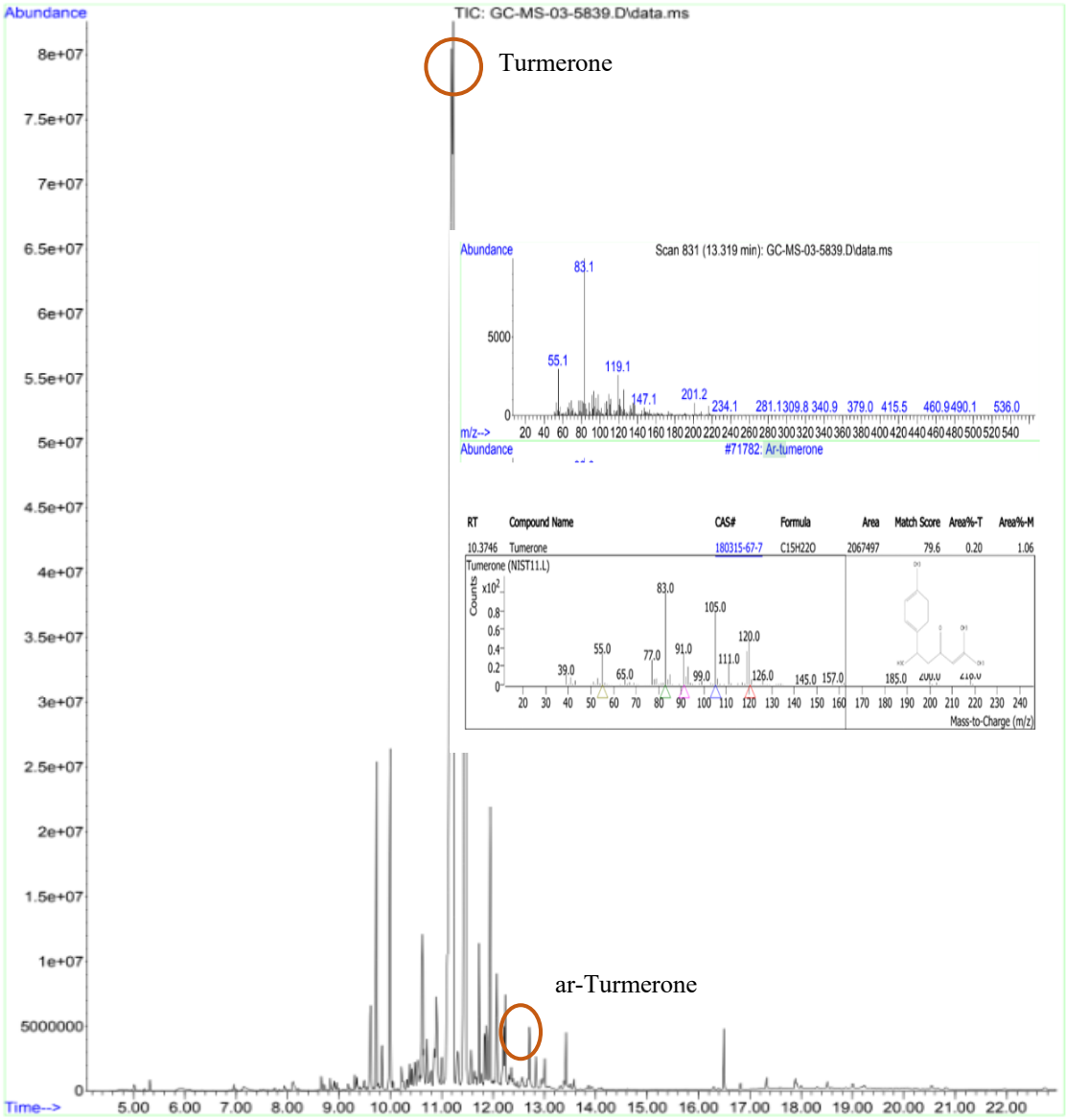

Fig. 8 – GC-MS Analysis: Dry Rhizome

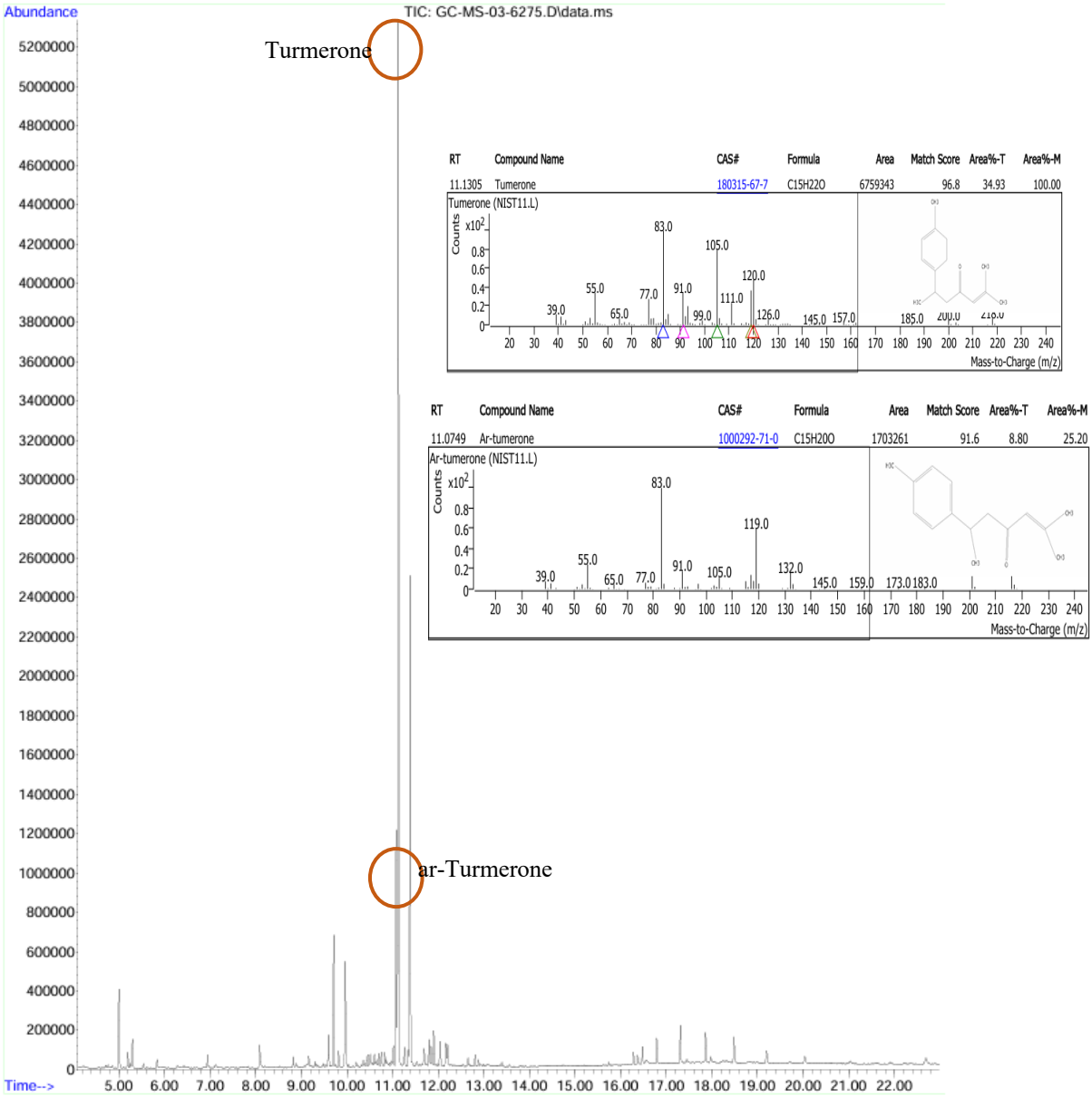

Fig. 9- GCMS Analysis – Fresh Rhizome

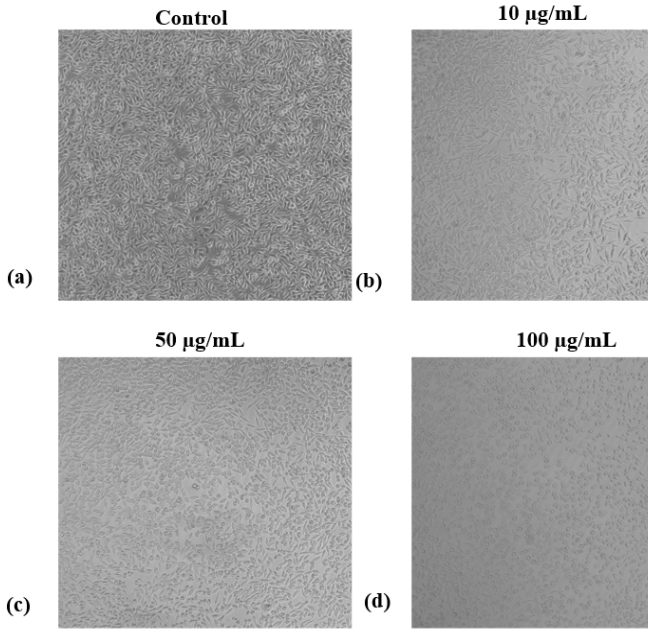

Fig. 10 - MTT Assay Analysis of Turmeric Oleoresin on L929 Cells (a) Control sample without treatment; (b) concentration of 10 µg/mL; (c) concentration of 50 µg/mL; and (d) concentration of 100 µg/mL

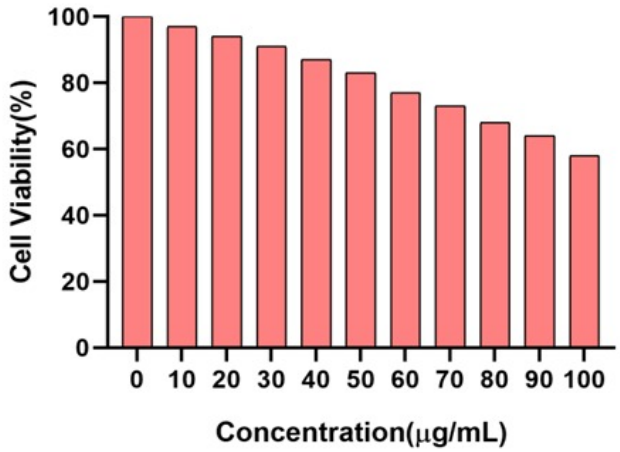

Fig.11-MTT assay on L929 cells showing dose-dependent reduction in cell viability

***In vitro* scratch assay**

The scratch assay is a standardized *in vitro* technique employed to quantitatively assess cellular migration and proliferation dynamics on two-dimensional substrates in response to experimental treatments. Confluent monolayers are mechanically disrupted using a sterile pipette tip to generate a linear wound gap, which is immediately imaged (time 0) and subsequently monitored at defined intervals. The extent of wound closure is quantified by calculating the percentage reduction of the scratch area relative to the initial gap.

In this investigation, the wound closure kinetics exhibited a temporally dependent pattern consistent with enhanced cell motility and mitotic activity. Initial imaging at 0 hours confirmed a well-defined acellular zone. At 12 hours post-scratch, partial re-epithelialization was observed, corresponding to approximately 35% gap closure. This progressed to 70% closure by 24 hours, and by 48 hours, the wound area was effectively sealed (~95% closure), indicating robust migratory and proliferative responses (Fig. 12). Fluorescence microscopy analysis demonstrated a concomitant increase in viable cell density within the wound region over time, supporting quantitative observations. These data underscore the cells' intrinsic regenerative capacity and substantiate the efficacy of the applied treatment in promoting cellular migration and proliferation critical to wound healing processes.

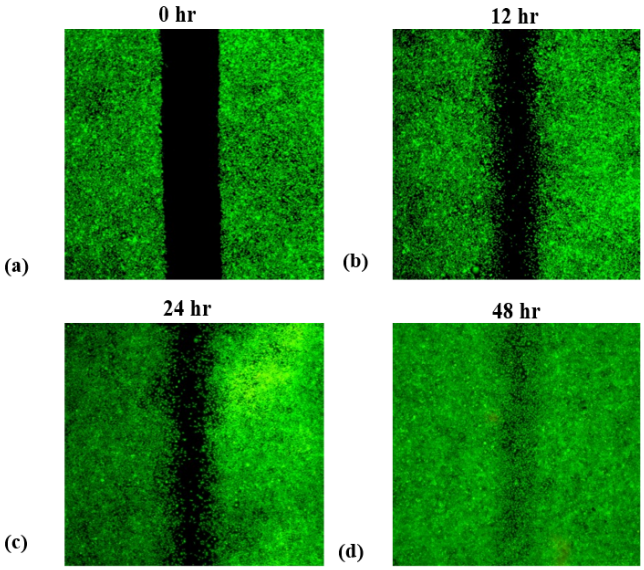

Fig. 12- Fluorescence Microscopy Images Depicting Wound Closure in L929 Cells Treated with Turmeric Oleoresin at different hours (a) 0 hr; (b) 12 hrs; (c) 24 hrs; and (d) 48 hrs

DISCUSSION

The present study builds upon existing research highlighting the diverse pharmacological potential of turmeric-derived phytoconstituents, particularly turmerone and ar-turmerone, and extends their evaluation to wound healing via MMP-9 inhibition. A previous investigation into Ar-turmerone identified it as a promising scaffold for dual inhibition of human acetylcholinesterase (AChE, PDB: 4PQE) and human

salivary α-amylase (PDB: 1XV8). In that study, Ar-turmerone demonstrated strong negative binding energies (−7.9 kcal/mol for AChE and −6.7 kcal/mol for α-amylase), attributed primarily to robust intra- and intermolecular hydrogen bonding interactions (35), (36). The compound also showed favorable ADMET properties, suggesting its potential for oral therapeutic use in treating neurological disorders and diabetes.

In comparison, the current research focused on the wound-healing potential of turmerone and ar-turmerone by targeting matrix metalloproteinase-9 (MMP-9) using *in silico* docking, MD simulations, and ADMET predictions. Among the two, turmerone demonstrated a significantly stronger binding affinity (−10.1 kcal/mol) relative to ar-turmerone (−8.1 kcal/mol), suggesting more stable interactions with MMP-9. This enhanced binding was likely due to π–π stacking interactions with the catalytic His401 residue and a more extensive van der Waals interaction network, consistent with known binding patterns of potent MMP-9 inhibitors, where turmerone showed significant binding energies in docking studies, indicating its potential as an MMP-9 inhibitor (37), (38).

Comparable interactions have been described with natural sesquiterpenes, where hydrophobic interactions were the major contributor to the stability of binding (39). MD simulations verified the stability of both complexes, with B-factor plots registering the slightest atomic fluctuations (Fig 6 & 7), whereas the elastic network model pointed towards enhanced rigidity in the MMP-9-turmerone complex, which would imply extended inhibitory activity—critical to the extent of extracellular matrix degradation reduction in chronic wounds (40). These observations are in agreement with recent data on ligand-induced stabilization of wound healing targets (41), (42). ADMET profiling revealed favorable drug-likeness for both compounds, adhering to Lipinski's Rule of Five (Table 1), with acceptable physicochemical properties such as logP < 5 and molecular weight < 500 Da, supported by SwissADME predictions (43). Toxicity analysis using ProTox 3.0 indicated low risk, with LD_{50} values > 2000 mg/kg (Table 3), consistent with previous studies on turmeric derivatives (44). The findings of this study suggest that Ar-Turmerone displayed better docking performance and stronger binding affinity than the standard drugs, which may be attributed to its effective hydrogen bonding interactions within and between molecules.

Experimental verification by GC-MS analysis proved the existence of turmerone (34.93%) and ar-turmerone (8.80%) in turmeric oleoresin (Fig. 8 and Fig 9), consistent with metabolomic accounts (45), and UV spectroscopy demonstrated characteristic absorption at 233 nm, consistent with curcuminoid chromophore patterns (46). These compounds are known for their significant biological activities, including anti-inflammatory, antioxidant, and anticancer effects, which support the therapeutic potential of turmeric oleoresin in various applications. This complementary analytical verification underscores the chemical stability and composition of the oleoresin, providing a biochemical basis for its observed biological activities. The similarity between GC-MS data enhances the reliability of our characterization and supports the potential utility of turmeric oleoresin as a natural bioactive agent in medicinal and nutraceutical formulations.

Based on these findings, fresh turmeric oleoresin was chosen for further biological evaluation, including the scratch wound healing test. The higher turmerone content in the fresh rhizome is expected to improve the oleoresin's therapeutic effects, especially in influencing MMP-9 activity and promoting tissue regeneration.

In vitro tests exhibited low cytotoxicity against L929 fibroblasts with $IC_{50} \geq 100$ µg/mL (Fig. 10), consistent with the reported pro-proliferative activity of turmeric (47). Scratch assays also verified increased cell migration at reduced concentrations (Fig.11), validating their function in wound closure, in line with fibroblast activation studies using natural compounds. The wound healing studies with turmeric oleoresin showcased significant enhancement in cellular migration and proliferation, achieving ~95% wound closure within 48 hours, indicating strong regenerative potential.

Overall, these results validate the therapeutic promise of turmerone and ar-turmerone as biocompatible MMP-9 inhibitors in wound healing processes (48), (49). Their ability to act as biocompatible MMP-9 inhibitors may further contribute to modulating extracellular matrix remodelling, essential for proper tissue repair. This positions these compounds as promising therapeutic candidates for enhancing wound healing processes, with the advantage of low toxicity and supportive biocompatibility. Future studies could focus on elucidating the molecular pathways involved and evaluating their efficacy in vivo, moving closer to clinical application.

CONCLUSION

The study highlights the potential of turmeric-derived compounds, Turmerone and Ar-Turmerone, in promoting wound healing through their strong inhibitory interaction with MMP-9. Molecular docking studies revealed high binding affinities, with Turmerone (-10.1) and Ar-Turmerone (-8.1), indicating their therapeutic significance. Both compounds also satisfy Lipinski's Rule of 5, suggesting good oral bioavailability. Toxicity predictions confirmed their safety, as they were inactive in all tested toxicity categories, including hepatotoxicity, nephrotoxicity, and cardiotoxicity. Molecular dynamics simulations also proved Turmerone-MMP-9 interactions to be stable, corroborating their efficacy as wound-healing agents. GC-MS analysis of turmeric rhizomes revealed Turmerone and Ar-Turmerone to be predominant constituents, further testifying to their natural abundance and viability for therapeutic use. *In vitro* assays offered further proof of their biocompatibility, with MTT assay results showing an IC_{50} of 100 µg/mL in L929 cells, affirming low cytotoxicity. Scratch assay findings revealed time-dependent wound healing with 95% healing at 48 hours, indicating strong cell migration and proliferation. The results indicate that turmeric oleoresin, which is a rich source of Turmerone and Ar-Turmerone, possesses huge potential for therapeutic applications in wound healing. Future research should focus on hydrogel formulations with these bioactives to maximize therapeutic effects in the clinic.

Conflict of Interest Statement

The authors declare that there is no conflict of interest regarding the publication of this manuscript.

REFERENCES

1. Młynarska E, Czarnik W, Dzieża N, Jędraszak W, Majchrowicz G, Prusinowski F, Stabrawa M, Rysz J & Franczyk B, Type 2 diabetes mellitus: new pathogenetic mechanisms, treatment and the most important complications. Int. J. Mol. Sci, 26 (2025) 1094.

2. Tönnies, T., Rathmann, W., Hoyer, A., Brinks, R., & Kuss, O. (2021). Quantifying the underestimation of projected global diabetes prevalence by the International Diabetes Federation (IDF) Diabetes Atlas. BMJ Open Diabetes Research & Care, 9(1), e002122.

3. Burgess JL, Wyant WA, Abujamra BA, Kirsner RS & Jozic I, Diabetic Wound-Healing Science. Medicina, 57 (2021) 1072.

4. Yang L, Rong GC & Wu QN, Diabetic foot ulcer: Challenges and future. World J Diabetes, 13 (2022) 1014.

5. Deng L, Du C, Song P, Chen T, Rui S, Armstrong DG & Deng W, The role of oxidative stress and antioxidants in diabetic wound healing. Oxid Med Cell Longev, 1 (2021) 8852759.

6. Tomic D, Shaw JE & Magliano DJ, The burden and risks of emerging complications of diabetes mellitus. Nat Rev Endocrinol, 18 (2022) 525.

7. Huang Y & Kyriakides TR, The role of extracellular matrix in the pathophysiology of diabetic wounds. Matrix Biol, 6 (2020), 100037.

8. Eming SA, Martin P & Tomic-Canic M, Wound repair and regeneration: Mechanisms, signaling, and translation. Sci Transl Med, 6 (2014) 3009337.

9. Bharathy P & Thanikachalam PV, Harnessing traditional herbal medicine: molecular insights into diabetic wound healing for modern therapeutics. Dig Chinese Med, 7 (2024) 388.

10. Chen J, Qin S, Liu S, Zhong K, Jing Y, Wu X, Peng F, Li D & Peng C, Targeting matrix metalloproteases in diabetic wound healing. Front Immunol 14, (2023) 1089001.

11. Cho H, Balaji S, Hone NL, Moles CM, Sheikh AQ, Crombleholme TM, Keswani SG & Narmoneva DA, Diabetic wound healing in a MMP9-/- mouse model. Wound Repair and Reg, 24 (2016) 829.

12. Cai F, Chen W, Zhao R & Liu Y, Mechanisms of Nrf2 and NF-κB pathways in diabetic wound and potential treatment strategies. Mol Biol Rep, 50 (2023) 5355.

13. Yang L, Rong GC & Wu QN, Diabetic foot ulcer: Challenges and future. World J Diabetes, 13 (2022) 1014.

14. Tejada S, Manayi A, Daglia M, Nabavi SF, Sureda A, Hajheydari Z, Gortzi O, Pazoki-Toroudi H & Nabavi SM, Wound Healing Effects of Curcumin: A short review. Curr Pharm Biotechnol, 17 (2016) 1002.

15. Thangapazham RL, Sharad S & Maheshwari RK, Phytochemicals in wound healing. Adv Wound Care, 5 (2014) 0505.

16. Kunnumakkara AB, Hegde M, Parama D, Girisa S, Kumar A, Daimary UD, Garodia P, Yenisetti SC, Oommen OV & Aggarwal BB, Role of Turmeric and Curcumin in Prevention and Treatment of Chronic Diseases: Lessons Learned from Clinical Trials. ACS Pharmacol Transl Sci, 6 (2023) 447.

17. Jangra N, Singla A, Puri V, Dheer D, Chopra H, Malik T & Sharma A, Herbal bioactive-loaded biopolymeric formulations for wound healing applications. RSC Adv, 15 (2025) 12402.

18. Qadir A, Jahan S, Aqil M, Warsi MH, Alhakamy NA, Alfaleh MA, Khan N & Ali A, Phytochemical-based nano-pharmacotherapeutics for management of burn wound healing. Gels, 7 (2021) 209.

19. Lipinski, C. A., Lombardo, F., Dominy, B. W., & Feeney, P. J. (2001). Experimental and computational approaches to estimate solubility and permeability in drug discovery and development settings .Advanced Drug Delivery Reviews 23 (1997) 3–25. 1. Advanced Drug Delivery Reviews, 46(1–3), 3–26.

20. Meng EC, Goddard TD, Pettersen EF, Couch GS, Pearson ZJ, Morris JH & Ferrin TE, UCSF ChimeraX: Tools for structure building and analysis. Prot Sci, 32 (2023) 4792.

21. Goddard TD, Huang CC, Meng EC, Pettersen EF, Couch GS, Morris JH, Ferrin TE, UCSF ChimeraX: Meeting modern challenges in visualization and analysis. Prot Sci, 27 (2017) 14.

22. Koshy CM, Asirvatham D, Majumdar R & Sugumar S, *In silico* Structural and Functional Characterization of a Hypothetical Protein from Stenotrophomonas maltophilia SRM01. J Pure Appl Microbiol, 16 (2022) 1167.

23. Daina A, Michielin O, Zoete V & Swiss, ADME: a free web tool to evaluate pharmacokinetics, drug-likeness and medicinal chemistry friendliness of small molecules. Sci Rep, 7 (2017) 42717.

24. Banerjee P, Kemmler E, Dunkel M & Preissner R, ProTox 3.0: a webserver for the prediction of toxicity of chemicals. Nucl Acids Res, 52 (2024) 513.

25. Dallakyan S & Olson AJ. Small-Molecule Library Screening by Docking with PyRx. Methods Mol Biol, (2014) 243.

26. Baroroh, Umi, M. Biotek, Zahra Silmi Muscifa, Wanda Destiarani, Fauzian Giansyah Rohmatullah, & Muhammad Yusuf, Molecular interaction analysis and visualization of protein-ligand docking using Biovia Discovery Studio Visualizer. Indonesian J Compl Biol, 2 (2023) 22.

27. López-Blanco JR, Aliaga JI, Quintana-Ortí ES & Chacón P, iMODS: internal coordinates normal mode analysis server. Nucl Acids Res 42 (2014) 271.

28. Gustini S, Hamdani S & Rinaldi K, Optimization of ar-Turmerone Isolation Method from Turmeric Oleoresin using Silica Gel Adsorbent. L. Appl. Nano Bio Sci, 12 (2022) 53.

29. Slaček G, Kotnik P, Osmić A, Postružnik V, Knez Ž, Finšgar M & Marevci MK, The Extraction Process, Separation, and Identification of Curcuminoids from Turmeric Curcuma longa. Foods, 12 (2023) 4000.

30. Ciuca MD & Racovita RC, Curcumin: overview of extraction methods, health benefits, and encapsulation and delivery using microemulsions and nanoemulsions. Int J Mol Sci, 24 (2023) 8874.

31. Singh S, Sankar B, Rajesh S, Sahoo K, Subudhi E & Nayak S, Chemical Composition of Turmeric Oil (Curcuma longa L.cv. Roma) and its Antimicrobial Activity against Eye Infecting Pathogens. J Ess Oil Res, 23 (2011) 11.

32. Fahmy NM, Fayez S, Uba AI, Shariati MA, Aljohani ASM, El-Ashmawy IM, Batiha GES, Eldahshan OA, Singab AN & Zengin G. Comparative GC-MS Analysis of Fresh and Dried Curcuma Essential Oils with Insights into Their Antioxidant and Enzyme Inhibitory Activities. Plants, 12 (2023) 1785.

33. Mosmann T, Rapid colorimetric assay for cellular growth and survival: Application to proliferation and cytotoxicity assays. J Imm Methods, 65 (1983) 55.

34. Martinotti, S., & Ranzato, E. (2019). Scratch wound healing assay. In Methods in molecular biology (pp. 225–229).

35. Shunmuga Priya V, Pradiba D, Aarthy M, Singh SK, Achary A & Vasanthi M, In-silico strategies for

identification of potent inhibitor for MMP-1 to prevent metastasis of breast cancer. J Biomol Struct Dyn, 39 (2021) 7274.

36. Liu N, Wang X, Wu H, Lv X, Xie H, Guo Z, Wang J, Dou G, Zhang C & Sun M. Computational study of effective matrix metalloproteinase 9 (MMP9) targeting natural inhibitors. Aging, 13 (2021) 22867.

37. Shaikh AS, Sethi A, Makhal PN, Rathi B & Kaki VR, Quest for selective MMP9 inhibitors: a computational approach. J Biomol Struct Dyn, 41 (2023) 15053.

38. Yusuf M, Pal S, Shahid M, Asif M, Khan SA & Tyagi R, Docking and ADMET Study of ArTurmerone: Emerging Scaffold for Acetylcholine Esterase Inhibition and Antidiabetic Target. J. Appl. Organometallic Chem, 3 (2023) 1.

39. Pradiba D, Aarthy M, Shunmugapriya V, Singh SK & Vasanthi M, Structural insights into the binding mode of flavonols with the active site of matrix metalloproteinase-9 through molecular docking and molecular dynamic simulations studies. J Biomol Struct Dyn, 36 (2018) 3718.

40. Shaikh AS, Sethi A, Makhal PN, Rathi B & Kaki VR, Quest for selective MMP9 inhibitors: a computational approach. J Biomol Struct Dyn, 41 (2023) 15053.

41. Lu W, Zhang J, Huang W, Zhang Z, Jia X, Wang Z, Shi L, Li C, Wolynes PG & Zheng S, Dynamic Bind: predicting ligand-specific protein-ligand complex structure with a deep equivariant generative model. Nat Comm, 15 (2024) 1071.

42. Jones JI, Nguyen TT, Peng Z & Chang M, Targeting MMP-9 in diabetic foot ulcers. Pharm, 12 (2019) 79.

43. Daina A, Michielin O & Zoete V, SwissADME: a free web tool to evaluate pharmacokinetics, drug-likeness and medicinal chemistry friendliness of small molecules. Sci rep, 7 (2017) 42717.

44. Balaji S & Chempakam B, Toxicity prediction of compounds from turmeric (Curcuma longa L). Food Chem Toxicol, 48 (2010) 2951.

45. Herebian D, Choi J, El-Aty AMA, Shim J & Spiteller M, Metabolite analysis in Curcuma domestica using various GC-MS and LC-MS separation and detection techniques. BMC, 23 (2009) 951.

46. Subhan MA, Alam K, Rahaman MS, Rahman MA & Awal R, Synthesis and Characterization of Metal Complexes Containing Curcumin and Study of their Anti-microbial Activities and DNA-binding Properties. J Sci Res, 6 (2013) 97.

47. Azzahra NF, Indrawati R & Diyatri I, Cytotoxicity of Turmeric Extract (Curcuma longa linn.) on BHK21 Fibroblast Cells. Int J Sci Soc, 6 (2024) 185.

48. Berry CE, Brenac C, Gonzalez CE, Kendig CB, Le T, An N & Griffin MF, Natural compounds and biomimetic engineering to influence fibroblast behavior in wound healing. Int J Mol Sci, 25 (2024) 3274.

49. Addis R, Cruciani S, Santaniello S, Bellu E, Sarais G, Ventura C, Maioli M & Pintore G. Fibroblast Proliferation and Migration in Wound Healing by Phytochemicals: Evidence for a novel synergic outcome. Int J Med Sci, 17 (2020) 1030.